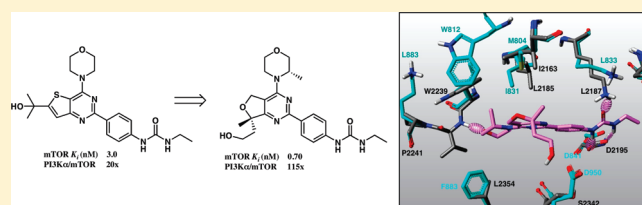


Potent, Selective, and Orally Bioavailable Inhibitors of Mammalian Target of Rapamycin (mTOR) Kinase Based on a Quaternary Substituted Dihydrofuropyrimidine

Frederick Cohen,^{*,†} Philippe Bergeron,[†] Elizabeth Blackwood,[‡] Krista K. Bowman,[§] Huifen Chen,[‡] Antonio G. DiPasquale,[○] Jennifer A. Epler,[‡] Michael F. T. Koehler,[†] Kevin Lau,[†] Cristina Lewis,^{||} Lichuan Liu,[#] Cuong Q. Ly,[†] Shiva Malek,^{||} Jim Nonomiya,^{||} Daniel F. Ortwine,[†] Zhonghua Pei,[†] Kirk D. Robarge,[†] Steve Sideris,^{||} Lan Trinh,^{||} Tom Truong,[‡] Jiansheng Wu,[▽] Xianrui Zhao,[†] and Joseph P. Lyssikatos[†][†]Department of Discovery Chemistry, [‡]Department of Translational Oncology, [§]Department of Structural Biology, ^{||}Department of Biochemical Pharmacology, [#]Department of Drug Metabolism and Pharmacokinetics, and [▽]Department of Protein Chemistry, Genentech, Inc., 1 DNA Way, South San Francisco, California 94080, United States[○]X-ray Crystallography Facility, University of California Berkeley, 32 Lewis Hall Berkeley, California 94720, United States

S Supporting Information

ABSTRACT: A series of inhibitors of mTOR kinase based on a quaternary-substituted dihydrofuropyrimidine was designed and synthesized. The most potent compounds in this series inhibited mTOR kinase with $K_i < 1.0$ nM and were highly ($>100\times$) selective for mTOR over the closely related PI3 kinases. Compounds in this series showed inhibition of the pathway and antiproliferative activity in cell-based assays. Furthermore, these compounds had excellent mouse PK, and showed a robust PK–PD relationship in a mouse model of cancer.



INTRODUCTION

The mammalian target of rapamycin (mTOR) signaling pathway serves as a central regulator of cell metabolism, growth, proliferation, and survival.^{1,2} The identification of mTOR as an essential downstream component of the PI3K/Akt signaling pathway provides a strong rationale for targeting mTOR in tumors harboring mutations or amplification of PI3K, Akt, or mutations or deletion of the PTEN phosphatase gene, a tumor suppressor that negatively regulates PI3K activity.³ mTOR is a serine–threonine protein kinase of the phosphoinositide 3-kinase (PI3K) superfamily, referred to as class IV PI3Ks, which resides in two distinct multiprotein complexes, mTOR complex-1 (mTORC1) and mTOR complex-2 (mTORC2).⁴ The mTORC1 complex is known for its critical role in protein synthesis and can phosphorylate 4EBP1 and S6K1, two key regulators of translation initiation, whereas mTORC2 functions as a key regulator of cell growth, metabolism, and survival and can phosphorylate Akt1. The natural product rapamycin and semisynthetic analogues selectively inhibit the activity of mTORC1 in an allosteric manner.⁵ Despite potent and selective inhibition of the mTORC1 complex, the clinical success of rapamycin has been limited to a few rare cancers. It has been suggested that this limited efficacy may be due to (1) lack of mTORC2 complex inhibition, (2) hyperactivation of PI3K signaling due to suppression of a negative feedback loop, and/or (3) partial inhibition of mTORC1 activity.³ Development of ATP-

competitive mTOR kinase inhibitors may circumvent many of these limitations, as this strategy enables potent inhibition of the mTORC1 and mTORC2 complexes and will allow for pharmacological validation of complete mTOR kinase inhibition in the clinic.

Our mTOR program began with compound 1, which was found to be a potent inhibitor of recombinant mTOR kinase ($K_i = 3$ nM) with $20\times$ selectivity versus PI3K α (Figure 1).⁶ The selectivity of this molecule was unique among this series and was attributed in large part to the ethyl urea substituent. Our efforts to improve the properties of this lead involved a number of heterocyclic A-rings. The knowledge gained from this effort led us to hypothesize that cyclic ethers would provide an optimal balance of properties. We synthesized a number of cyclic ethers such as 3–5. Molecular modeling suggested that a small hydrophobic group above the plane of the inhibitor at the 7-position would provide additional selectivity over the PI3 kinases, while blocking a benzylic position through quaternization was expected to reduce metabolism. These considerations brought us to conceptual compound 6. A search of the literature revealed known β -keto ester 7 as a likely precursor to compounds such as 6.⁷

RESULTS AND DISCUSSION

Although β -keto ester 7 was readily prepared, conversion to the corresponding uracil by direct condensation with urea⁸ or

Received: February 24, 2011

Published: April 15, 2011

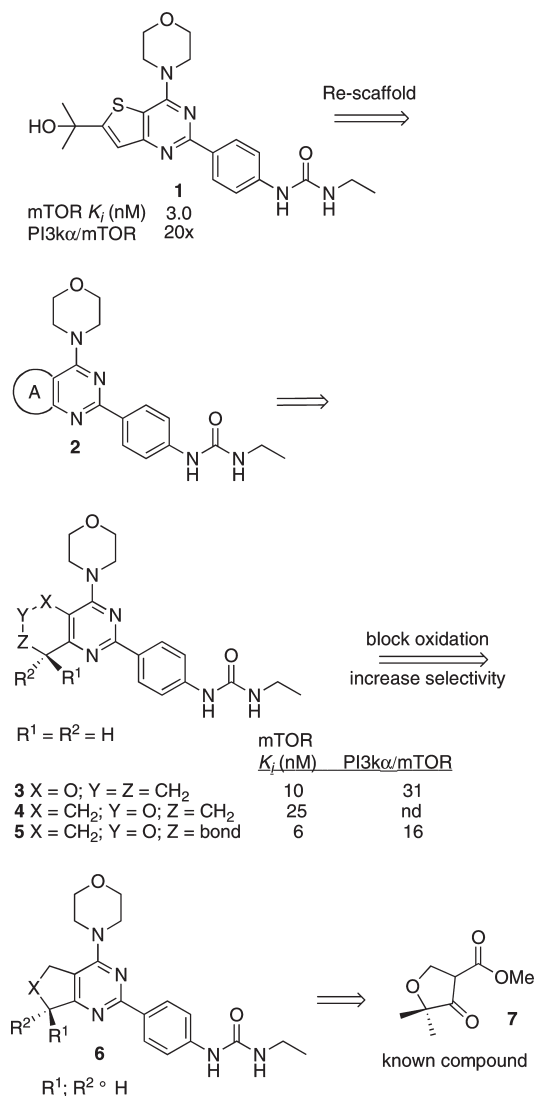


Figure 1. Design strategy for geminal-disubstituted dihydrofuroprymidine scaffold.

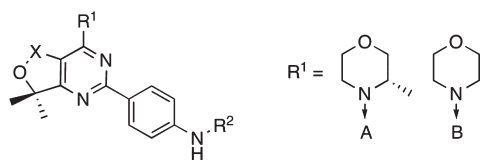
thiourea⁹ failed to afford any identifiable products. Condensation with a benzamidine also failed.¹⁰ Since such reactions worked well in our hands on other substrates, we attributed this lack of reactivity to steric hindrance of the ketone by the neighboring quaternary center. We were able to condense β -keto ester **7** with ammonia to provide enamine **8** in good yield (Scheme 1).¹¹ Reaction of this enamine with COCl₂, pyridine, and then ammonia provided a urea intermediate, which cyclized to uracil **9** under gentle heating. The crude uracil was heated in a mixture of POCl₃ and 1,2-dichloroethane to provide dichloropyrimidine **10**. The inhibitors were completed using standard transformations.

In vitro potencies of these compounds were measured against recombinant mTOR kinase domain using a LanthaScreen FRET assay, and against PI3K α and PI3K δ using a fluorescence polarization assay as previously described.⁶ Activity in a cellular context was assessed by measuring the inhibition of phosphorylation of two known mTOR substrates, Akt (serine 473) and p70S6K in a pTEN-null prostate carcinoma NCI-PC3 cell line. Antiproliferative activity was determined in a 3-day viability assay using NCI-PC3 and MCF7 neo/HER2 cell lines. Results

from these assays are summarized in Table 1. In general, these compounds were very potent mTOR inhibitors, generally with K_i < 5 nM, and were highly selective for mTOR over the PI3 kinases. There were a few notable exceptions to this trend. We observed (as have others)¹² that removal of the methyl group from the morpholine leads to a significant loss in selectivity (Table 1, compare **13b** with **13c**). We also observed that replacement of the ethyl group on the urea with a small heterocycle (**13a** vs **13g**) led to a significant loss in selectivity for PI3K α but not for PI3K δ , a trend that we observed in other scaffolds (data not shown). Since the urea substituent was predicted by MetaSite¹³ to be a hot spot for CYP-mediated metabolism, significant effort went into its replacement (Supporting Information Table S1). The only substituent we found that maintained potency and selectivity was a pyridone (**13i**). This group was predicted by modeling to retain significant hydrogen bonding interactions with the mTOR protein. Polar compounds such as **13h** (TPSA = 129; cLogP = 1.4 compare to **13a**, TPSA = 88; cLogP = 2.8), made in an attempt to increase metabolic stability, maintained potency in the enzymatic assays, but potency in cell-based assays was significantly reduced.

Compounds from this series were predicted to have moderate to high clearance (Cl) in humans, rats, and mice, with rates of >50% of liver blood flow, based on in vitro liver microsome data. (Table 2). When the pharmacokinetic (PK) properties were measured in mice, we observed a good correlation (within 2 \times) between predicted and observed Cl. Our hopes for pyridone **13i** as a urea replacement were dashed by its low oral bioavailability (7%). When dosed in rats, we observed Cl rates much higher than predicted. For example, **13a** and **13d** had Cl rates of 44 and 55 (mL/min)/kg, respectively. Since the urea substituent seemed to have little effect on either in vitro or in vivo metabolic stability, we turned our attention to the other side of the molecule. The benzylic position was predicted to be a primary spot of metabolism, both by first principles¹⁴ and by MetaSite.¹³ Thus, we removed it by oxidation to lactones **13b** and **13c**. However, this had no effect on in vitro or in vivo stability (Table 2).

As we had exhausted our options for reasonable modifications of the gem-dimethyl scaffold, we sought to redesign it in a manner that would allow introduction of additional structural diversity. Our criterion was rapid access to a versatile intermediate without a large increase in molecular weight. Switching one of the methyl groups to allyl seemed to satisfy the criterion. The synthesis (Scheme 2) began by condensation of allyl substituted α -hydroxy ester **14**¹⁵ with ethyl acrylate to provide β -ketoester **15** along with a number of byproducts that were not readily separated. Impure **15** was condensed with ammonia to provide **16**, which was readily purified in 50% yield for the two steps. The dichloropyrimidine ring was completed as described in Scheme 1. The allyl group was then elaborated as described in Schemes 2 and 3, with reference to Table 3. Finally, all racemates or diastereomeric pairs were resolved by chiral stationary phase HPLC. The stereochemistry of the quaternary center in **22d** was unambiguously assigned as *R* by X-ray crystallographic analysis (see Supporting Information). In most cases one diastereomer or enantiomer was significantly more potent (in either the biochemical or cell-based assay) and/or selective than the other. Since the structural basis for these trends was consistent with predictions from molecular modeling studies (vide infra), we assigned the chirality of the remaining analogues by analogy. The exceptions were the pairs **21a/b** and **23a/b**, where the stereochemistry of the quaternary center remained ambiguous. As in

Table 1. Structure and Potency of gem-Dimethyl Scaffold^a


The main structure shows a bicyclic core with a morpholine ring fused to a pyridine ring. The pyridine ring has a gem-dimethyl group at position 2, a substituent R¹ at position 3, and a para-substituted phenyl ring at position 4. The phenyl ring has an NH-R² group. R¹ is defined as either a morpholine ring (A) or a piperazine ring (B). R² is defined as either a carbonyl group (A) or a carbonyl group with a substituent (B).

Compd	R ²	R ¹ /X	potency/selectivity		target modulation ^b		proliferation	
			mTor K _i (nM)	PI3K α / δ (fold)	pAkt IC ₅₀ (nM)	pp70S6K IC ₅₀ (nM)	NCI- PC3 IC ₅₀ (nM)	MCF7neo/Her2 IC ₅₀ (nM)
13a		A/CH ₂	1.4	120/290	4.6	13	78	52
13b		A/CO	1.2	85/320	7.6	13	60	220
13c		B/CO	2.6	40/110	16	20	120	310
13d		A/CH ₂	1.6	47/110	4.0	4.8	46	66
13e		A/CH ₂	3.2	61/77	26	30	120	260
13f		A/CH ₂	3.0	120/200	37	30	160	480
13g		A/CH ₂	0.80	14/230	4.3	6.0	52	160
13h		A/CH ₂	3.6	24/54	37	47	330	1900
13i		A/CH ₂	1.2	180/510	9.3	15	120	120

^a Assays described in ref 6. ^b Assayed in NCI-PC3 cell line.

Table 2. PK Profiles of gem-Dimethyl Scaffold

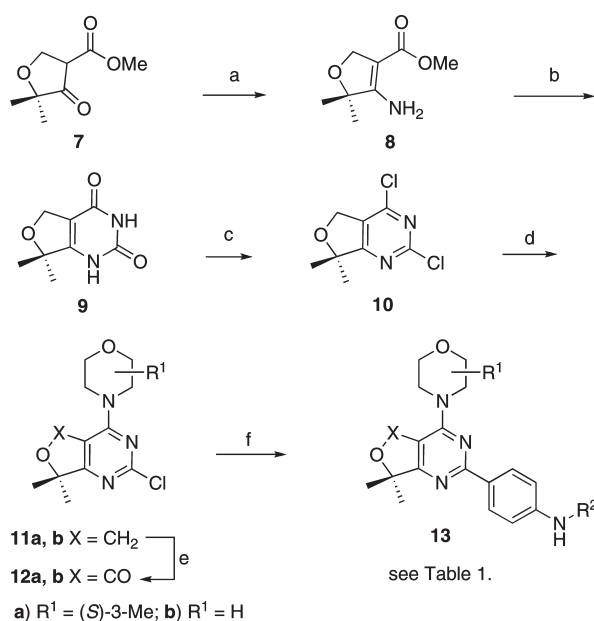
compd	microsome Cl _{hep} ^b (mL/min)/kg h/r/m ^c	mouse PK ^a					
		iv (1 mg/kg)			po (5 mg/kg)		PPB (%) h/r/m ^c
		Cl (mL/min)/kg	V _{ss} (L/kg)	t _{1/2} (h)	AUC (μM·h)	F (%)	
13a	18/27/53	46	1.4	0.40	6.1	140	86/92/95
13d	14/25/49	53	1.5	0.42	0.81	22	72/70/81
13i	15/29/50	44	1.9	2.2	0.31	7	98/96/97
13c	13/28/56	30	0.57	0.21	1.5	23	98/95/98
13b	18/21/57						
13e	16/26/43						
13f	15/23/44						
13g	16/17/38						
13h	11/18/47						

^a Compound dosed iv as a solution in 80%PEG/10%EtOH and dosed po as a suspension in MCT. ^b Cl_{hep} predicted from incubation with microsomes. ^c h/r/m = human/rat/mouse.

the dimethyl analogues, most of these elaborated compounds were potent, with mTOR K_i < 5 nM, and highly selective for mTOR over the PI3 kinases. Potency in the enzymatic assay translated well to potency in substrate phosphorylation and proliferation cellular assays. Similar to findings with the structural

modifications in the ether ring, or on the urea, substitution at the quaternary center led to no improvement in metabolic stability, either in vitro or in vivo. (Table 4).

Molecular Modeling Studies. To help rationalize the observed SAR and assist in the design of potent, selective analogues, a homology model of the mTOR kinase domain was built from a PI3Kγ crystal structure and selected compounds were examined by docking.¹⁶ Consistent with reported modeling analyses, we observed that analogues with substituents on the morpholine ring conferred higher selectivity for mTOR over the PI3 kinases. The mTOR-selective bridged bicyclomorpholine analogues **22c** and **22f** fill the larger cavity predicted for this region in mTOR because of a Leu2354 to Phe961 (PI3Kγ numbering) swap (Figure 2).¹² In addition, there is predicted to be a small hydrophobic pocket adjacent to the inhibitor morpholine formed primarily by the Trp2239 residue (Ile881 in PI3Kγ). In addition to its larger size compared with that of Ile, this Trp is predicted to be held rigidly in place in the mTOR protein because of a Pro residue two amino acids upstream (Lys883 in PI3Kγ) that imparts increased rigidity to the mTOR protein in this region relative to PI3Kγ. The 3-methyl group on the morpholine of compounds such as **13a** fits well in this pocket, packing against the Trp, without significantly disturbing the predicted Trp conformation. This is consistent with the high potency and selectivity observed for these 3-methylmorpholine analogues.

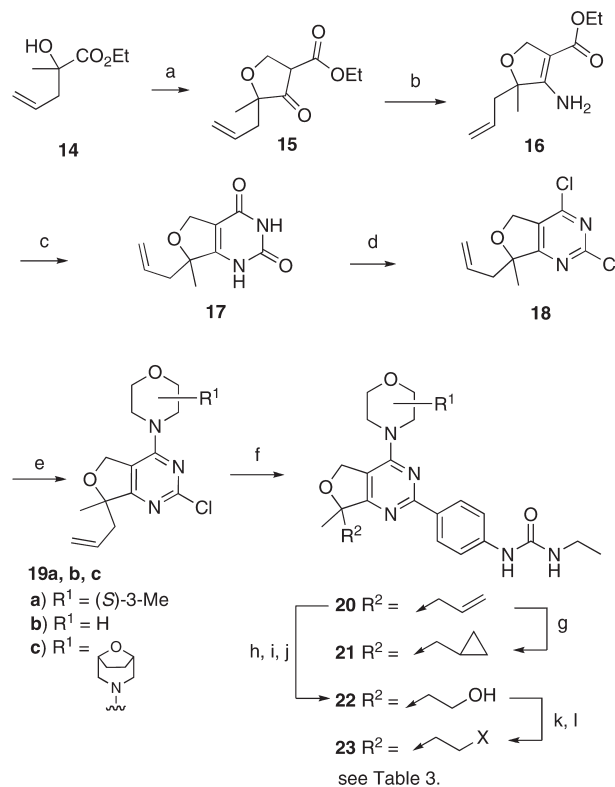
Scheme 1. Synthesis of gem-Dimethyl Dihydrofuropyrimidines^a

^a Reagents and conditions: (a) NH₄OAc, MeOH, reflux 70%; (b) COCl₂, pyridine, CH₂Cl₂, then NH₄OH, then reflux; (c) POCl₃, 1,2-dichloroethane 65%, two steps; (d) morpholine or (S)-3-methylmorpholine, DIPEA, DMF; (e) PhIO, KBr, montmorillonite K10, water, MeCN 80%; (f) (RO)₂BC₆H₄N(H)R², (Ph₃P)₄Pd, base, MeCN, water, Δ.

Another region of variability between mTOR and PI3Kγ proteins involves Leu2185 (Ile831 in PI3Kγ) and Ile2160 (Met804 in PI3Kγ). Taken together, these branched alkyl residues in mTOR, in addition to Pro2169 (also Pro810 in PI3Kγ), combine to create a small hydrophobic patch above the plane of the inhibitor bicyclic ring system as shown in Figure 2B. This region is well-suited to interact with small alkyl groups such as the methyl group of analogues such as 22a. The hydroxyethyl group of 22a is predicted to extend away from this site toward the Ser2342 residue in mTOR (Asp950 in PI3Kγ). These potential interactions may explain the increased potency and selectivity observed for the S-configured 22a and allowed us to assign the stereochemistry of most of the analogues in this series by analogy.

Finally, in the back pocket of the binding site, the urea portion of inhibitors such as 13a and 22a is predicted to form three hydrogen bonds, two to Asp841 and one to Lys833, effectively locking this portion of the inhibitor in place. In the region adjacent to the urea, mTOR presents a Glu2190 from the C-helix (Asp836 in PI3Kγ). This Glu residue in mTOR is predicted to orient in a way that exposes the hydrophobic ethylene portion of its side chain directly toward the ethyl substituent on the urea. The corresponding Asp in PI3Kγ cannot adopt a similar conformation, resulting in a more open, polar site in this area that is less tolerant of a hydrophobic substituent on the urea. Thus, the ethylurea provides the optimal combination of mTOR potency and selectivity versus the PI3 kinases.

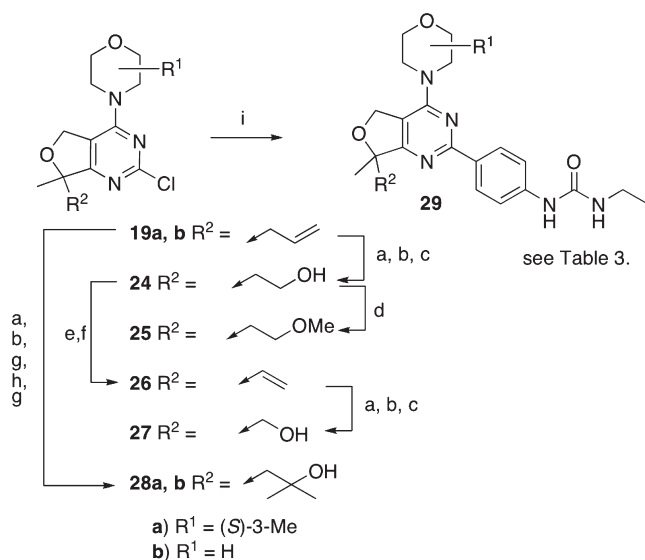
The C-helix is flexible in the kinase family, and such flexibility certainly clouds the detailed explanation of observed potency differences between mTOR and PI3K families. However, these hypotheses have proven consistent in explaining observed potency differences among known inhibitors and have been used in

Scheme 2. Synthesis of Quaternary Substituted Analogues^a

^a Reagents and conditions: (a) NaH, then ethyl acrylate, DMSO; (b) NH₄OAc, EtOH, Δ, 50%, two steps; (c) COCl₂, pyridine, 1,2-dichloroethane, then NH₄OH, then Δ 22%; (d) POCl₃, 1,2-dichloroethane, Δ 75%; (e) morpholine, DIPEA, DMF 92%; (f) (RO)₂BC₆H₄N(H)Et, (Ph₃P)₄Pd, base, MeCN, water, Δ; (g) CH₂I₂, Et₂Zn, PhMe, Δ; (h) cat. OsO₄, N-methylmorpholine N-oxide, THF, water; (i) NaIO₄, THF, water; (j) NaBH₄, THF, MeOH, 60%; (k) MsCl, DIPEA, CH₂Cl₂; (l) XH, solvent, heat.

the design of urea replacements in this and other related series of mTOR inhibitors (data not shown).

To determine the dose- and time-dependent effects of these potent and selective inhibitors on mTOR pathway signaling *in vivo*, three dose levels of compounds 13a and 22a were administered to female NCR.nude mice bearing subcutaneous NCI-PC3 prostate tumors. Plasma and tumor samples were collected at 1, 6, and 10 h postdose and analyzed for drug exposure and PD target modulation. The NCI-PC3 cell line is PTEN-null, and as a consequence, the PI3K/Akt/mTOR signaling axis is activated in this tumor model and has been shown to be sensitive to rapamycin and mTOR kinase inhibitors alike.¹⁷ As illustrated in Figure 3, pS6RP (mTORC1 readout) and pAkt (mTORC2 readout) levels in this model were significantly reduced following treatment, with the maximum inhibition scoring at ~15–25% the baseline levels of Akt or pS6RP of baseline (time-matched vehicle controls). The combination of potency and high exposure of these molecules appears to result in maximal inhibition of the pathway at early time points, even at the lowest dose examined. However, partial recovery of the pAkt phospho marker is evident at later times, in a dose-dependent manner, despite drug exposures well in excess of the cellular IC₅₀ at all time points. Similar observations have been made in *in vitro* and *in vivo* studies of mTOR inhibitors.^{18,19}

Scheme 3. Further Elaboration of Quaternary Substituted Analogues^a

^a Reagents and conditions: (a) cat. OsO₄, *N*-methylmorpholine *N*-oxide, THF, water; (b) NaIO₄, THF, water; (c) NaBH₄, THF, MeOH; (d) NaH, MeI, THF; (e) MsCl, DIPEA, CH₂Cl₂; (f) KO-*t*-Bu, THF, 77%; (g) MeMgBr, THF; (h), Swern oxidation; (i) (RO)₂BC₆H₄N(H)Et, (Ph₃P)₄Pd, base, MeCN, water, Δ.

CONCLUSIONS

We designed and synthesized a series of potent and selective mTOR inhibitors. The most potent compounds from this series have mTOR K_i < 1 nM and >100× selectivity over the PI3Kα and PI3Kδ. These compounds were also very potent in anti-proliferative assays with IC₅₀ < 100 nM. Furthermore, these compounds had moderate Cl and high oral bioavailability in mice. The combination of good potency and high plasma exposure leads to significant knock-down of the pathway in a murine model of cancer at moderate doses. Further efficacy studies in murine models and selection of a clinical candidate will be reported in due course.

EXPERIMENTAL SECTION

All chemicals were purchased from commercial suppliers and used as received. Flash chromatography was carried out with prepacked silica cartridges from either ISCO or SiliCycle on an ISCO Companion chromatography system using gradient elution. NMR spectra were recorded on a Bruker AV III 400 or 500 NMR spectrometer and referenced to tetramethylsilane. Preparative HPLC was performed on a Polaris C₁₈ 5 μm column (50 mm × 21 mm), eluting with mixtures of water–acetonitrile. Low-resolution mass spectra were recorded on a Sciex 15 mass spectrometer in ES+ mode. High-resolution mass spectra were recorded on Waters LCT Premiere XC in ES+ mode. Diagnostic data are provided for intermediates that are mixtures of diastereomers. All final compounds were purified to >95% chemical and optical purity, as assayed by HPLC (Waters Acquity UPLC column, 21 mm × 50 mm, 1.7 μm) with a gradient of 0–90% acetonitrile (containing 0.038% TFA) in 0.1% aqueous TFA, with UV detection at λ = 254 and 210 nm, and with CAD detection with an ESA Corona detector. In cases where enantiomers or diastereomers were separated by chiral stationary phase HPLC, the final products were ≥98% ee or de.

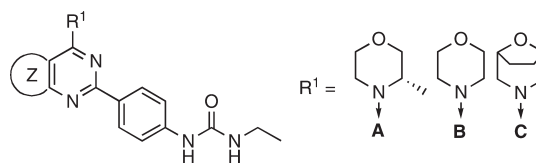
Methyl 4-Amino-5,5-dimethyl-2,5-dihydrofuran-3-carboxylate (8). A solution of methyl 5,5-dimethyl-4-oxodihydrofuran-3-carboxylate (7) (19.1 g, 111 mmol), ammonium acetate (89 g, 1.15 mol), and methanol (225 mL) was heated at reflux for 20 h. The solvent was removed under reduced pressure and the residue partitioned between saturated NaHCO₃ (500 mL) and ethyl acetate (150 mL). The phases were separated, and the aqueous phase was extracted with ethyl acetate (2 × 150 mL). The combined organic phases were washed with brine (1 × 50 mL), dried (Na₂SO₄), filtered, and concentrated onto Celite to afford a free-flowing powder. The residue was chromatographed: 330 g column, 5–30% ethyl acetate–heptane to afford 12.34 g (65%) 7 as a colorless solid: ¹H NMR (400 MHz, CDCl₃) δ 5.35 (s, 2H), 4.66 (s, 2H), 3.71 (s, 3H), 1.37 (s, 6H); ¹³C NMR (101 MHz, CDCl₃) δ 166.23, 162.47, 90.77, 84.85, 69.73, 50.47, 25.72; HRMS (ES+) *m/z* 172.0936 (172.0974 calcd for C₈H₁₄NO₃ M + H⁺).

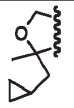
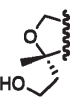
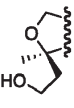
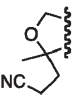
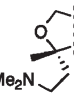
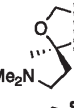
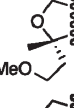
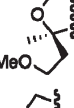
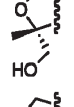
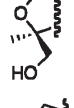


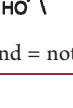
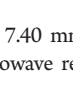


7,7-Dimethyl-5,7-dihydrofuro[3,4-*d*]pyrimidine-2,4(1*H*,3*H*)-dione (9). To a cool (0 °C) solution of 8 (12.34 g, 72.1 mmol), pyridine (23.3 mL, 288 mmol), and 1,2-dichloroethane (250 mL) was added phosgene (20% in toluene, 50 mL, 86.5 mmol) in one portion. The mixture was maintained at 0 °C for 3 h. Then 28% NH₄OH (80 mL) was added cautiously down the side of the flask and the mixture was stirred gently for 3 h, then heated at 50 °C for 16 h. Water (200 mL) was added, and the phases were separated. The organic phase was extracted with 1% NH₄OH (2 × 100 mL). The combined aqueous phases were washed with dichloromethane (3 × 20 mL) and concentrated to approximately 150 mL, which caused the product to precipitate. The precipitate was collected on paper, rinsed with a small amount water, and dried under high vacuum to afford 8.27 g of 9 as colorless crystals. Further concentration of the mother liquor provided a second crop of product, 1.07 g (71% combined yield): ¹H NMR (400 MHz, DMSO-*d*₆) δ 11.43 (s, 1H), 11.00 (s, 1H), 4.64 (s, 2H), 1.38 (s, 6H); ¹³C NMR (101 MHz, DMSO-*d*₆) δ 160.07, 157.69, 152.64, 104.56, 83.86, 67.76, 25.42; HRMS (ES+) *m/z* 183.0770 (183.0770 calcd for C₈H₁₁N₂O₃ M + H⁺).

2,4-Dichloro-7,7-dimethyl-5,7-dihydrofuro[3,4-*d*]pyrimidine (10). A mixture of 9 (2.55 g, 14.0 mmol), phosphoryl chloride (15 mL, 160 mmol), and 1,2-dichloroethane (80 mL) was heated at 80 °C for 20 h. The mixture was concentrated under reduced pressure at 40 °C to a solid which was dissolved in dichloromethane (250 mL) and saturated NaHCO₃ (500 mL). The phases were separated, and the aqueous phase was extracted with dichloromethane (3 × 50 mL). The combined organic phases were dried (Na₂SO₄), filtered, and concentrated to afford 2.53 g (82%) of 10 as a colorless solid: ¹H NMR (400 MHz, CDCl₃) δ 5.06 (s, 2H), 1.56 (s, 6H); ¹³C NMR (126 MHz, CDCl₃) δ 179.63, 160.63, 155.43, 127.64, 85.39, 66.89, 26.12; HRMS (ES+) *m/z* 219.0092 (219.0092 calcd for C₈H₉Cl₂N₂O M + H⁺).

(S)-2-Chloro-7,7-dimethyl-4-(3-methylmorpholino)-5,7-dihydrofuro[3,4-*d*]pyrimidine (11a). To a cool (0 °C) solution of 10 (2.53 g, 11.5 mmol), DIPEA (4.8 mL, 28 mmol), and DMF (15 mL) was added (S)-3-methylmorpholine (1.42 g, 14 mmol). The solution was allowed to warm slowly over 15 h. The solution was poured into saturated NH₄Cl (100 mL) and extracted with ether (3 × 50 mL). The combined organic phases were washed with brine (1 × 25 mL), dried (MgSO₄), filtered, and concentrated to afford 3.18 g (95%) of the title compound as a colorless solid: ¹H NMR (400 MHz, CDCl₃) δ 5.10 (d, *J* = 11.3 Hz, 1H), 5.05 (d, *J* = 11.3 Hz, 1H), 4.11 (brs, 1H), 3.99 (m, 2H), 3.72 (m, 2H), 3.55 (ddd, *J* = 11.9, 11.9, 2.8 Hz, 1H), 3.39 (ddd, *J* = 13.0, 13.0, 3.2 Hz, 1H), 1.47 (s, 3H), 1.46 (s, 3H), 1.36 (d, *J* = 6.8 Hz, 3H); ¹³C NMR (101 MHz, CDCl₃) δ 176.19, 160.18, 158.57, 108.03, 83.96, 70.73, 68.89, 66.81, 48.36, 40.10, 26.19, 26.10, 15.03; HRMS (ES+) *m/z* 284.1165 (284.1166 calcd for C₁₃H₁₉ClN₃O M + H⁺).

(S)-1-(4-(7,7-Dimethyl-4-(3-methylmorpholino)-5,7-dihydrofuro[3,4-*d*]pyrimidin-2-yl)phenyl)-3-ethylurea (13a). A mixture of 11a (1.65 g, 5.66 mmol), [4-ethylureido]phenylboronic acid pinacol ester (2.87 g, 9.90 mmol), tetrakis(triphenylphosphine)palladium(0) (440 mg, 0.38 mmol), 1.0 M Na₂CO₃ (7.4 mL, 7.40 mmol), 1.0 M

Table 3. Structure and Potency of Quaternary Substituted Analogues^a


compd	Z	R ¹	potency/selectivity		target modulation ^b		proliferation	
			mTor <i>K_i</i> (nM)	PI3K α / δ (fold)	pAkt IC ₅₀ (nM)	pp70S6K IC ₅₀ (nM)	NCI-PC3 IC ₅₀ (nM)	MCF7neo/Her2 IC ₅₀ (nM)
21a		A	1.0	98/200	2.8	5.0	31	95
21b		A	1.3	45/250	5.0	10	100	340
22a		A	0.70	115/415	1.6	1.7	15	15
22b		B	0.34	148/610	2.2	2.6	16	48
22c		C	0.66	844/8300	1.4	1.9	17	22
22d		A	4.0	94/228	19	40	118	510
22e		B	2.9	131/350	23	47	210	490
22f		C	1.0	2040/5300	28	27	66	160
23a		A	1.1	120/180	8.3	14	41	100
23b		A	1.3	64/200	11	15	74	193
23c		A	7.0	177/500	51	42	220	1100
23d		A	62	38/65	nd	nd	nd	nd
29a		A	1.7	380/1040	12	15	62	130
29b		A	7.9	63/145	41	69	284	1200
29c		A	1.7	210/280	11	12	95	192
29d		B	4.4	110/510	32	30	220	280
29e		A	6.8	6.0/6.6	48	77	450	530
29f		B	21	31/110	140	234	960	1700
29g		A	2.3	69/250	4.4	6.3	18	75
29h		B	1.8	60/350	11	7.2	28	27
29i		A	3.2	19/140	19	24	130	29
29j		B	4.7	22/240	43	41	140	170

^a Assays described in ref 6. nd = not determined. ^b Assayed in NCI-PC3 cell line.

potassium acetate (7.4 mL, 7.40 mmol), and acetonitrile (15 mL) was heated at 110 °C in a microwave reactor for 30 min. The mixture was

partitioned between saturated NH₄Cl (100 mL) and ethyl acetate (50 mL). The phases were separated and the aqueous phase was extracted with ethyl

Table 4. PK Profiles of Quaternary Substituted Analogues

compd	microsomes Cl_{hep}^b (mL/min)/kg h/r/m ^c	mouse PK ^a					PPB (%) h/r/m ^c
		iv (1 mg/kg)		po (5 mg/kg)			
		Cl (mL/min)/kg	V_{ss} (L/kg)	$t_{1/2}$ (h)	AUC (μ M·h)	F (%)	
22b	21/24/53	40	1.5	0.71	0.96	56	78/76/83
22a	15/24/61	64	1.5	0.33	0.59	110	87/nd/94
22c	17/25/67	47	2.0	0.77	0.78	50	73/74/89
22d	12/15/52	87	2.4	0.34	0.43	65	86/79/94
23c	10/34/74	76	2.6	0.57	0.14	6.0	59/67/78
29g	15/24/61	57	1.3	1.1	0.63	53	82/78/91
29h	13/29/59	55	1.0	0.27	0.66	55	77/79/86
29i	14/17/54	56	2.7	1.3	0.65	73	66/88/85

^a Compound dosed iv as a solution in 80% PEG/10% EtOH and dosed po as a suspension in MCT. ^b Cl_{hep} predicted from incubation with microsomes. ^c h/r/m = human/rat/mouse.

acetate (2 × 50 mL). The combined organic phases were dried (Na_2SO_4), filtered, adsorbed onto Celite, and chromatographed using an 80 g column and 0–75% ethyl acetate in heptane to afford 2.12 g of **13a** as a colorless solid with 90% purity. A portion of this material (0.50 g) was slurried in *i*-PrOH (5 mL) at 50 °C for 1 h. The material was collected by filtration on paper, washed with *i*-PrOH, and dried under vacuum to afford 325 mg of pure material: ¹H NMR (500 MHz, DMSO-*d*₆) δ 8.67 (s, 1H), 8.20 (d, *J* = 8.7 Hz, 2H), 7.48 (d, *J* = 8.8 Hz, 2H), 6.18 (t, *J* = 5.5 Hz, 1H), 5.15 (d, *J* = 11.7 Hz, 1H), 5.08 (d, *J* = 11.7 Hz, 1H), 4.27 (s, 1H), 3.99 (s, 1H), 3.93 (dd, *J* = 11.4, 3.3 Hz, 1H), 3.72 (d, *J* = 11.5 Hz, 1H), 3.65 (dd, *J* = 11.5, 2.8 Hz, 1H), 3.50 (ddd, *J* = 11.8, 11.8, 2.8 Hz, 1H), 3.38–3.32 (m, 1H), 3.17–3.04 (m, 2H), 1.40 (s, 3H), 1.39 (s, 3H), 1.26 (d, *J* = 6.8 Hz, 3H), 1.06 (d, *J* = 7.2 Hz, 3H); ¹³C NMR (126 MHz, DMSO-*d*₆) δ 173.48, 162.60, 157.39, 154.82, 142.65, 130.21, 128.33, 116.83, 106.87, 82.90, 70.21, 68.52, 66.21, 47.22, 33.87, 26.28, 26.23, 15.33, 14.21; HRMS (ES+) *m/z* 412.2272 (412.2349 calcd for C₂₂H₃₀N₅O₃ M + H⁺).

(±)-Ethyl 5-Allyl-4-amino-5-methyl-2,5-dihydrofuran-3-carboxylate (**16**). To a suspension of sodium hydride (1.9 g, 49 mmol) in THF (50 mL) was added ethyl 2-hydroxy-2-methylpent-4-enoate¹⁵ (7.0 g, 2.78 mol) at 0 °C under N₂, and the brown solution was stirred at 0 °C for 30 min and at room temperature for 30 min. The solvent was removed under reduced pressure to afford an oil, which was cooled at 0 °C. Ethyl acrylate (14 mL, 129 mmol) in DMSO (50 mL) was added rapidly. The ice bath was removed after 15 min, and the solution was stirred at room temperature for 1.5 h. The reaction mixture was poured into 3% H₂SO₄ (700 mL) slowly at 0 °C, followed by extraction with ether (3 × 150 mL). The combined organic phases were washed with brine, dried over MgSO₄, and concentrated to afford 9.40 g of β -keto ester (**15**) as a clear liquid, which was used without further purification.

The crude β -keto ester from above (9.40 g, 44 mmol) was combined with NH₄OAc (34 g, 443 mmol) and EtOH (200 mL) and heated at 85 °C overnight. The solvent was removed under reduced pressure, and the residue was diluted with EtOAc (250 mL). The precipitate was filtered and washed with EtOAc. The combined organics were washed with 10% NaHCO₃ (1 × 150 mL), brine (1 × 150 mL), dried over MgSO₄, filtered, and concentrated under reduced pressure. The residue was purified by flash chromatography, 220 g column, 1–15% EtOAc/heptane, to give 4.7 g (51%, two steps) of the title compound as a light-yellow oil. ¹H NMR (500 MHz, CDCl₃) δ 5.82 (ddd, *J* = 17.3, 10.2, 7.2 Hz, 1H), 5.55–5.25 (m, 1H), 5.18–5.05 (m, 2H), 4.74–4.57 (m, 2H), 4.24–3.98 (m, 2H), 2.49–2.22 (m, 2H), 1.37 (s, 3H), 1.27 (t, *J* = 7.1 Hz, 3H); ¹³C NMR (126 MHz, CDCl₃) δ 165.99, 161.04, 132.94, 118.85,

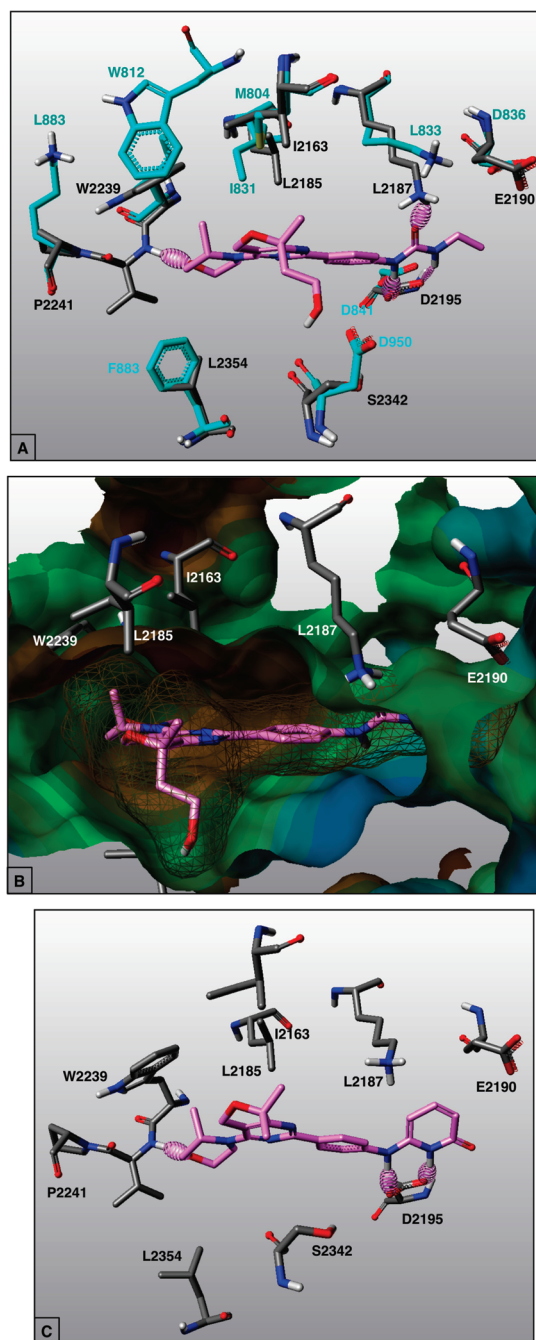


Figure 2. (A) Depiction of **22a** (pink) in the active site of the mTOR homology model with residues important for binding and selectivity vs PI3K γ shown in cyan. View is edge-on to the plane of the inhibitor bicyclic ring. Hydrogen bonds to the protein are shown as thick hashed lines. The image was generated using Benchware3DExplorer. (B) Same view and molecule as in (A) but with a vdW surface color-coded by lipophilic potential (tan-brown = lipophilic, cyan-blue = polar, green = between lipophilic and polar) added to the protein and with a mesh surface also color-coded by lipophilic potential added to the ligand to show shape and lipophilic complementarity. Note the brown regions match up with each other. (C) Docked model of pyridone **13i** showing conserved hydrogen bonds (Tripos Associates, St. Louis, MO).

91.98, 87.11, 70.85, 59.30, 43.95, 24.52, 14.70; HRMS (ES+) *m/z* 212.1276 (212.1287 calcd for C₁₁H₁₈NO₃ M + H⁺).

(±)-7-Allyl-7-methyl-5,7-dihydrofuran[3,4-*d*]pyrimidine-2,4(1*H*,3*H*)-dione (**17**). Phosgene (20% solution in toluene, 50.7 mL,

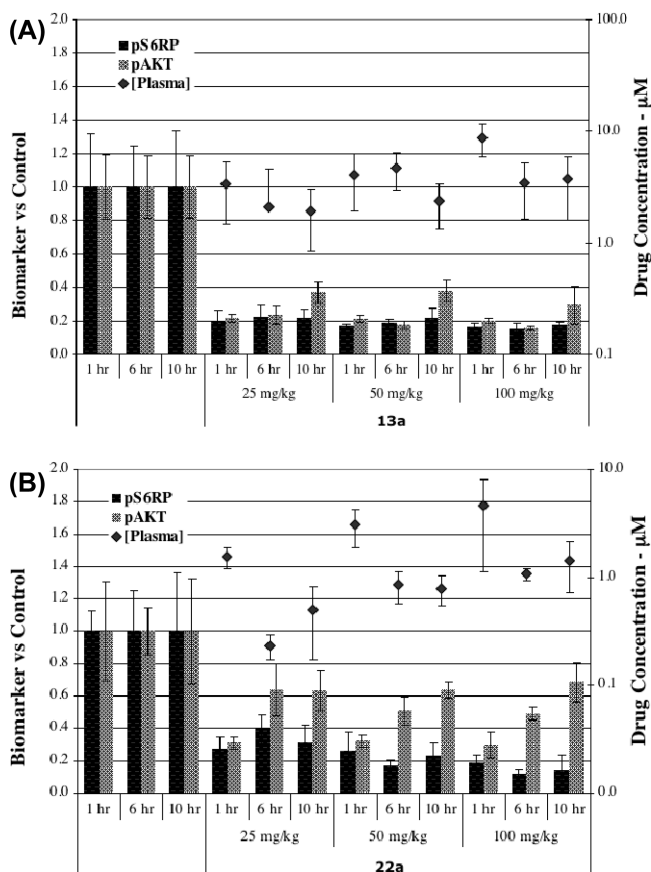


Figure 3. In vivo target modulation of mTOR pathway in NCI-PC3 human prostate tumor xenografts. Compounds **13a** (A) and **22a** (B) were administered as a single oral dose to tumor-bearing mice. Plasma and tumor samples were collected at 1, 6, and 10 h postdose and analyzed for drug exposure and PD biomarker modulation. Target inhibition was calculated relative to the average time-matched vehicle control.

95.8 mmol) was added to a solution of enamine **16** (13.5 g, 63.9 mmol), pyridine (20.7 mL, 256 mmol), and 1,2-dichloroethane (230 mL) at 0 °C over 10 min. After the addition, the ice bath was removed and the mixture was stirred at room temperature for 2 h. The reaction mixture was cooled in an ice bath, and NH_4OH (89 mL, 639 mmol) was added dropwise. After 15 min, the ice bath was removed and the mixture was allowed to warm to room temperature and then heated in an oil bath at 50 °C overnight. The mixture was allowed to cool to room temperature, and the phases were separated. The organic phase was extracted with 1% NH_4OH (2 × 100 mL). The combined aqueous phases were washed with CH_2Cl_2 (2 × 100 mL). The aqueous phase was concentrated under reduced pressure until solid precipitated. The solid was collected by filtration, washed with a small amount of water (20 mL), and dried under high vacuum to afford 5.9 g (44%) of the title compound as a light-yellow solid: ^1H NMR (500 MHz, $\text{DMSO}-d_6$) δ 10.99 (s, 1H), 5.74–5.56 (m, 1H), 5.09–5.02 (m, 2H), 4.66 (d, $J = 10.5$ Hz, 1H), 4.61 (d, $J = 10.5$ Hz, 1H), 3.28 (s, 1H), 2.55–2.51 (m, 1H), 2.42 (dd, $J = 14.3, 6.8$ Hz, 1H), 1.38 (s, 3H); ^{13}C NMR (126 MHz, $\text{DMSO}-d_6$) δ 159.84, 156.04, 152.52, 132.74, 118.47, 105.50, 86.41, 68.88, 42.47, 24.34. LC–MS: $m/z = 209$ ($\text{M} + \text{H}^+$).

(±)-7-Allyl-2,4-dichloro-7-methyl-5,7-dihydrofuro[3,4-*d*]pyrimidine (18). A suspension of **17** (5.9 g, 28 mmol), 1,2-dichloroethane (20 mL), and POCl_3 (35 mL, 375 mmol) was heated in a glass tube sealed with a Teflon screw-cap at 90 °C overnight. After cooling to room temperature, the reaction mixture was poured into crushed ice

(300 mL), made basic (pH ~ 9) by adding NaOH pellets (few at a time) while cooling in an ice bath. The dark brown basic mixture was extracted with CH_2Cl_2 (3 × 100 mL). The combined organic phases were dried over MgSO_4 , filtered, and concentrated under reduced pressure to afford 5.8 g (85%) of the title compound as a dark brown solid: ^1H NMR (500 MHz, CDCl_3) δ 5.69 (ddd, $J = 17.7, 10.4, 7.3$ Hz, 1H), 5.10–5.03 (m, 4H), 2.59 (d, $J = 7.3$ Hz, 2H), 1.51 (d, $J = 5.8$ Hz, 3H); ^{13}C NMR (101 MHz, $\text{DMSO}-d_6$) δ 178.32, 158.87, 154.53, 132.34, 128.97, 119.09, 86.73, 67.21, 43.31, 24.22. LC–MS: $m/z = 246$ ($\text{M} + \text{H}^+$).

7-Allyl-2-chloro-7-methyl-4-((S)-3-methylmorpholino)-5,7-dihydrofuro[3,4-*d*]pyrimidine (19a). Compound **19a** was prepared from intermediate **18** by the procedure for compound **11a**: ^1H NMR (500 MHz, CDCl_3) δ 5.76–5.66 (m, 1H), 5.11–5.02 (m, 4H), 3.98 (dd, $J = 11.6, 3.6$ Hz, 1H), 3.73 (m, 2H), 3.56 (t, $J = 11.8$ Hz, 1H), 3.56 (t, $J = 11.8$ Hz, 1H), 3.37 (t, $J = 12.7$ Hz, 1H), 3.37 (t, $J = 12.7$ Hz, 1H), 2.60–2.47 (m, 2H), 1.45 (s, 3H), 1.34 (m, 3H). LC–MS: $m/z = 310$ ($\text{M} + \text{H}^+$).

1-(7-Allyl-7-methyl-4-((S)-3-methylmorpholino)-5,7-dihydrofuro[3,4-*d*]pyrimidin-2-yl)phenyl)-3-ethylurea (20a). Compound **20a** was prepared from intermediate **19a** by the procedure for compound **13a**: ^1H NMR (400 MHz, CDCl_3) δ 8.37 (d, $J = 8.6$ Hz, 2H), 7.37 (d, $J = 8.7$ Hz, 2H), 6.38 (s, 1H), 5.83–5.71 (m, 1H), 5.19–4.99 (m, 4H), 4.74 (s, 1H), 4.24–4.12 (m, 1H), 4.07–4.00 (m, 2H), 3.82–3.74 (m, 2H), 3.62 (ddd, $J = 11.9, 11.9, 2.8$ Hz, 1H), 3.42 (ddd, $J = 12.6, 12.6, 2.7$ Hz, 1H), 3.37–3.29 (m, 2H), 2.65–2.53 (m, 2H), 1.50 (s, 3H), 1.36 (t, $J = 6.7$ Hz, 3H), 1.18 (t, $J = 7.2$ Hz, 3H). LC–MS: $m/z = 438$ ($\text{M} + \text{H}^+$).

1-Ethyl-3-(4-((S)-7-(2-hydroxyethyl)-7-methyl-4-((S)-3-methylmorpholino)-5,7-dihydrofuro[3,4-*d*]pyrimidin-2-yl)phenyl)urea (22a) and 1-Ethyl-3-(4-((R)-7-(2-hydroxyethyl)-7-methyl-4-((S)-3-methylmorpholino)-5,7-dihydrofuro[3,4-*d*]pyrimidin-2-yl)phenyl)urea (22d). Olefin **20a** (100 mg, 0.2 mmol) was dissolved in THF/water (3:1, 6 mL) and cooled in an ice bath. To this solution was added *N*-methylmorpholine *N*-oxide (32 mg, 0.27 mmol) and OsO_4 (a couple crystals). The resulting solution was stirred at room temperature for 48 h. It was quenched by the addition of Na_2SO_3 (340 mg, 2.7 mmol), stirred at room temperature for 30 min, diluted with water (10 mL), and extracted with EtOAc (2 × 20 mL). The combined organic phases were dried over MgSO_4 , filtered, and concentrated under reduced pressure to afford a crude diol, which was carried on without further purification. LC–MS: $m/z = 472$ ($\text{M} + \text{H}^+$).

The crude diol from above was dissolved in THF/water (3:1, 6 mL), and NaIO_4 (73 mg, 0.34 mmol) was added in one portion. The mixture was stirred at room temperature for 1.5 h. The reaction mixture was diluted with brine (10 mL), and the aqueous layer was extracted with EtOAc (2 × 20 mL). The combined organic phases were dried over MgSO_4 , filtered, and concentrated under reduced pressure to afford crude aldehyde, which was carried on without further purification. LC–MS: $m/z = 442$ ($\text{M} + \text{H}^+$).

The aldehyde from above was dissolved in THF (2 mL) with a few drops of MeOH added. The mixture was cooled in an ice bath, and NaBH_4 (17 mg, 0.46 mmol) was added. The resulting mixture was stirred at room temperature for 30 min. The reaction was quenched with the addition of saturated aqueous NH_4Cl (5 mL), and the aqueous layer was extracted with EtOAc (2 × 20 mL). The combined organic phases were dried over MgSO_4 , filtered, and concentrated under reduced pressure. The residue was purified by Prep HPLC to afford 60 mg of as white solid. A 40 mg portion of this material was purified by SFC Chiralpak As-H, 25% MeOH in CO_2 , to afford 23.3 mg (60%) of **22d** as a white solid and 16.3 mg (40%) of **22a** as a white solid: (**22d**) ^1H NMR (400 MHz, $\text{DMSO}-d_6$) δ 8.65 (s, 1H), 8.20 (d, $J = 8.8$ Hz, 2H), 7.48 (d, $J = 8.8$ Hz, 2H), 6.14 (t, $J = 5.6$ Hz, 1H), 5.16 (d, $J = 11.7$ Hz, 1H), 5.06 (d, $J = 11.7$ Hz, 1H), 4.33 (t, $J = 5.3$ Hz, 1H), 4.24 (s, 1H), 3.94 (d, $J = 8.3$ Hz, 2H), 3.68 (dt, $J = 11.7, 7.2$ Hz, 2H), 3.53–3.48 (m, 2H), 3.33 (s, 1H), 3.17–3.07 (m, 2H), 2.01–1.91 (m, 2H), 1.37 (s, 3H), 1.25 (d, $J = 6.7$ Hz, 3H), 1.06 (t, $J = 7.2$ Hz, 3H); ^{13}C NMR (126 MHz, $\text{DMSO}-d_6$) δ

172.42, 162.48, 157.34, 154.77, 142.65, 130.13, 128.32, 116.80, 108.84, 107.32, 84.31, 70.16, 69.26, 66.17, 56.76, 47.21, 42.31, 33.85, 25.34, 15.32, 14.17; HRMS (ES+) m/z 442.2493 (442.2454 calcd for $C_{23}H_{31}N_5O_4 M + H^+$); (22a) 1H NMR (400 MHz, DMSO- d_6) δ 8.65 (s, 1H), 8.20 (d, $J = 8.8$ Hz, 2H), 7.48 (d, $J = 8.8$ Hz, 2H), 6.14 (t, $J = 5.7$ Hz, 1H), 5.11 (q, $J = 11.7$ Hz, 2H), 4.33 (t, $J = 5.3$ Hz, 1H), 4.24 (s, 1H), 3.94 (d, $J = 8.0$ Hz, 2H), 3.72 (d, $J = 10.9$ Hz, 1H), 3.65 (d, $J = 8.8$ Hz, 1H), 3.58–3.47 (m, 2H), 3.32 (s, 1H), 3.11 (dd, $J = 13.5$, 6.4 Hz, 2H), 1.95 (d, $J = 9.2$ Hz, 2H), 1.37 (s, 3H), 1.25 (d, $J = 6.7$ Hz, 3H), 1.06 (t, $J = 7.1$ Hz, 3H); HRMS (ES+) m/z 442.2462 (442.2454 calcd for $C_{23}H_{32}N_5O_4 M + H$).

Molecular Modeling. A homology model of the mTOR kinase domain was built from publicly available PI3K γ crystal structures (PDB code 3IBE) using the Fugue and Orchestrate modules of Sybyl, version 8.1 (Tripos Associates, St. Louis, MO), and further optimized using the Maximin module within Sybyl (all atoms, AmberFF02 charges on protein, MMFF94 charges on ligand) including the bound ligand from 3IBE. Docking studies were conducted using Gold, version 4.1, with a single hydrogen bond constraint to the hinge Val backbone NH, allowing flexible Lys and Asp side chains so appropriate hydrogen bond geometry between the ligand urea moiety and protein could be attained. A 10 Å sphere around the centroid of the ligand was used to define the active site region.

In-Life PK–PD Study. Human prostate cancer NCI-NCI-PC3 cells (National Cancer Institute, Frederick, MD) were implanted subcutaneously into the right hind flanks of female NCR.nude mice (5×10^6 cells in 100 μ L of Hank's balanced salt solution). Tumors were monitored until they reached a mean tumor volume of approximately 500 mm³. Then similarly sized tumors were randomly assigned to groups ($n = 4$). Compounds 13a and 22a were formulated as suspensions in 0.5% methylcellulose/0.2% Tween 80 (MCT) and dosed orally at 25, 50, and 100 mg/kg (100 μ L dose/25 g animal). Tumor and plasma samples were harvested at 1, 6, and 10 h postdose.

Blood samples were harvested by terminal cardiac puncture and collected into tubes containing K₂EDTA as an anticoagulant. Samples were kept chilled on ice until centrifugation at (1500–2000)g for 5 min; plasma was transferred to a new vial and snap frozen. Tumor samples were transferred to a 1.5 mL snap-cap polypropylene tube, weighed, and then flash frozen on dry ice. Samples were stored at –80 °C prior to PD biomarker evaluation.

Xenograft Tumor Lysates. Frozen tumors were lysed in ice-cold extraction buffer by mechanical disruption and agitation with garnet/ceramic sphere matrix in a FastPrep-24 (MP Biomedicals, Solon, OH; five 20 s cycles with rest periods on wet ice). Extraction buffer (Biosource; Carlsbad, CA) was supplemented with protease inhibitors (F. Hoffman-La Roche; Mannheim, Germany), 1 mM phenylmethylsulfonyl fluoride, and phosphatase inhibitor cocktails 1 and 2 (Sigma-Aldrich; St. Louis, MO). After thorough disruption, tumor lysates were clarified by centrifugation at 4 °C. Protein concentrations were determined using the BCA protein assay kit (Pierce; Rockford, IL) and normalized to a standard concentration of 5 mg/mL.

PD Biomarker Assays. The Meso Scale Discovery Multi-Spot biomarker detection system (Meso Scale Discovery; Gaithersburg, MD) was used to determine the levels of Akt phosphorylated at serine 473 (pAkt) and S6RP phosphorylated at serine 235/236 (pS6RP). These double-determinant immunoassays quantify protein levels on the basis of measurements of electrochemoluminescence intensity. In the case of pS473 and total Akt, both of these were measured in the same well using a duplex assay plate. All other markers required separate plates to measure phosphorylated and total protein. Protein was loaded at 20 μ g/well for Akt and 10 μ g/well for S6RP.

Relative levels of phosphoprotein were determined by comparison of treated tumor lysates with an average of the time-matched vehicle controls.

■ ASSOCIATED CONTENT

S Supporting Information. Structures of additional mTOR inhibitors, additional experimental procedures, 1H NMR spectra, and X-ray data collection and analysis results. This material is available free of charge via the Internet at <http://pubs.acs.org>.

■ AUTHOR INFORMATION

Corresponding Author

*Phone: 650-225-1000. Fax: 650-467-8922. E-mail: fcohen@gene.com

■ ACKNOWLEDGMENT

We thank members of the DMPK and Purification groups within Genentech Small Molecule Drug Discovery for analytical support.

■ ABBREVIATIONS USED

mTOR, mammalian target of rapamycin; PI3K, phosphatidylinositol 3 kinase; mTORC, mammalian target of rapamycin complex; LC–MS, liquid chromatography–mass spectrometry; TPSA, topological polar surface area; PPB, plasma protein binding; PTEN, phosphatase and tensin homologue; CYP, cytochrome P450

■ REFERENCES

- (1) Wullschleger, S.; Loewith, R.; Hall, M. N. TOR signaling in growth and metabolism. *Cell* **2006**, *124*, 471–484.
- (2) Chiang, G.; Abraham, R. T. Targeting the mTOR signaling network in cancer. *Trends Mol. Med.* **2007**, *13*, 433–442.
- (3) Liu, Q.; Thoreen, C.; Wang, J.; Sabatini, D.; Gray, N. S. mTOR mediated anti-cancer drug discovery. *Drug Discovery Today: Ther. Strategies* **2009**, *6*, 47–55.
- (4) Guertin, D. A.; Sabatini, D. M. The pharmacology of mTOR inhibition. *Sci. Signaling* **2009**, *2*, pe24.
- (5) Sudarsanam, S.; Johnson, D. E. Functional consequences of mTOR inhibition. *Curr. Opin. Drug Discovery Dev.* **2010**, *13*, 31–40.
- (6) Sutherlin, D. P.; Sampath, D.; Berry, M.; Castanedo, G.; Chang, Z.; Chuckowree, L.; Dotson, J.; Folkes, A.; Friedman, L.; Goldsmith, R.; Heffron, T.; Lee, L.; Lesnick, J.; Lewis, C.; Mathieu, S.; Nonomiya, J.; Olivero, A.; Pang, J.; Prior, W.; Salphati, L.; Sideris, S.; Tian, Q.; Tsui, V.; Wan, N. C.; Wang, S.; Wiesmann, C.; Wong, S.; Zhu, B.-Y. Discovery of (thienopyrimidin-2-yl)aminopyrimidines as potent, selective, and orally available pan-PI3-kinase and dual pan-PI3-kinase/mTOR inhibitors for the treatment of cancer. *J. Med. Chem.* **2010**, *53*, 1086–1097.
- (7) Gianturco, M. A.; Friedel, P. A synthesis of 2,2,4-trimethyl-4-hydroxytetrahydrofuran, a product of the photolysis of 4-methyl-4-pentanone. *Can. J. Chem.* **1965**, *43*, 2121–2122.
- (8) Nakai, H.; Saito, T.; Obitsu, T. CRF Antagonists and Heterobicyclic Compounds. EP 1666468, 2006.
- (9) Danel, K.; Larsen, E.; Pedersen, E. B. An easy synthesis of 5,6-disubstituted acylclouridine derivatives. *Synthesis* **1995**, 934–936.
- (10) Wang, J.; Zhang, Y.; Gonzales, J. E., III; Martinborough, E.; Zimmerman, N. Condensed Pyrimidine Compounds as Inhibitors of Voltage-Gated Ion Channels. WO 200514558, 2005.
- (11) Tang, W.; Wu, S.; Zhang, X. Enantioselective hydrogenation of tetrasubstituted olefins of cyclic β -(acylamino)acrylates. *J. Am. Chem. Soc.* **2003**, *125*, 9570–9571.
- (12) Zask, A.; Kaplan, J.; Verheijen, J. C.; Richard, D. J.; Curran, K.; Brooijmans, N.; Bennett, E. M.; Toral-Barza, L.; Hollander, I.; Ayril-Kaloustian, S.; Yu, K. Morpholine derivatives greatly enhance the selectivity of mammalian target of rapamycin (mTOR) inhibitors. *J. Med. Chem.* **2009**, *52*, 7942–7945.

(13) Cruciani, G.; Carosati, E.; De Boeck, B.; Ethirajulu, K.; Mackie, C.; Howe, T.; Vianello, R. MetaSite: understanding metabolism in human cytochromes from the perspective of the chemist. *J. Med. Chem.* **2005**, *48*, 6970–6979.

(14) King, R. S. Biotransformations in Drug Metabolism. In *Drug Metabolism Handbook*; Nassar, A. F., Hollenberg, P. F., Scatina, J., Eds.; John Wiley & Sons, Inc.: Hoboken, NJ, 2009; pp 17–38.

(15) Ojima, I.; Miyazawa, Y.; Kumagi, M. Asymmetric addition of allyltrimethylsilane to (–)-menthyl pyruvate and phenylglyoxylate. *J. Chem. Soc., Chem. Commun.* **1976**, 927–928.

(16) Nowak, P.; Cole, D. C.; Brooijmans, N.; Bursavich, M. G.; Curran, K. J.; Ellingboe, J. W.; Gibbons, J. J.; Hollander, I.; Hu, Y.; Kaplan, J.; Malwitz, D. J.; Toral-Barza, L.; Verheijen, J. C.; Zask, A.; Zhang, W.-G.; Yu, K. Discovery of potent and selective inhibitors of the mammalian target of rapamycin (mTOR) kinase. *J. Med. Chem.* **2009**, *52*, 7081–7089.

(17) Grunwald, V.; DeGraffenried, L.; Russel, D.; Friedrichs, W. E.; Ray, R. B.; Hidlago, M. Inhibitors of mTOR reverse doxorubicin resistance conferred by PTEN status in prostate cancer cells. *Cancer Res.* **2002**, *62*, 6141–6145.

(18) Javle, M. M.; Shroff, R. T.; Xiong, H.; Varadhachary, G. A.; Fogelman, D.; Reddy, S. A.; Davis, D.; Zhang, Y.; Wolff, R. A.; Abbruzzese, J. L. Inhibition of the mammalian target of rapamycin (mTOR) in advanced pancreatic cancer: results of two phase II studies. *BMC Cancer* **2010**, 368–375.

(19) Breuleux, M.; Klopfenstein, M.; Stephan, C.; Doughty, C. A.; Barys, L.; Maira, S. M.; Kwiatkowski, D.; Lane, H. A. Increased AKT S473 phosphorylation after mTORC1 inhibition is rictor dependent and does not predict tumor cell response to PI3K/mTOR inhibition. *Mol. Cancer Ther.* **2009**, *8*, 742–753.